Journal of Nano- and Electronic Physics
Vol. **14** No 5, 05020(6pp) (2022)

Журнал нано- та електронної фізики
Том **14** № 5, 05020(6cc) (2022)

Electrical Conduction and Polarization Properties of InSe<$CS(NH_2)_2$<$C_{14}H_{10}$>> Clathrate

V. Maksymych[1], D. Calus[2], D. Matulka[1], P. Chabecki[2], R. Shvets[1], N. Pokladok[1], F. Ivashchyshyn[1,2]

[1] *Institute of Applied Mathematics and Fundamental Sciences, Lviv Polytechnic National University, 12, Bandera St., 79013 Lviv, Ukraine*
[2] *Faculty of Electrical Engineering, Czestochowa University of Technology, 69, ul. J.H. Dąbrowskiego, 42-201 Częstochowa, Poland*

(Received 30 August 2022; revised manuscript received 24 October 2022; published online 28 October 2022)

InSe<$CS(NH_2)_2$<$C_{14}H_{10}$>> clathrate is a 2D hierarchical structure of the subhost<host<guest>> type obtained by the intercalation method under the influence of light. In this case, we used a layered InSe single crystal as a semiconductor 2D matrix, thiourea ($CS(NH_2)_2$) functioned as a supramolecular cavitand, and anthracene ($C_{14}H_{10}$) as a photoelectret. We used illumination during synthesis for the photoelectret polarization of anthracene. The impedance spectroscopy method was used to study the conductive and polarization properties of InSe<$CS(NH_2)_2$<$C_{14}H_{10}$>> clathrate. As a result, the manifestation of photoinduced quantum capacitance was recorded, the nature of which is associated with the discretization of the energy spectrum and finite tunneling times. The results obtained from the study of the thermally stimulated discharge spectra show that InSe<$CS(NH_2)_2$<$C_{14}H_{10}$>> clathrate is characterized by homo-charge relaxation and broad bands with a quasi-continuous spectrum of localized states. The behavior of the current-voltage characteristics indicates the manifestation of photocurrent with a value of + 23.5 mV.

Keywords: InSe, Thiourea, Anthracene, Clathrate, Impedance spectroscopy, Quantum capacitance, Photocurrent.

DOI: 10.21272/jnep.14(5).05020 PACS numbers: 72.80.Jc, 82.75. – z

1. INTRODUCTION

Progress in electronics development, namely reducing its size and providing functional hybridity, increasingly encourages researchers to search for new heterostructured nanomaterials. For this purpose, various technological approaches are being developed for the synthesis of inorganic/inorganic, organic/inorganic, and bio/inorganic nanohybrids, which have unique electrophysical properties due to the manifestation of quantum-size effects [1-4]. A broad range of synthetic technological approaches, such as vacuum deposition, photolithography, chemical vapor deposition, Langmuir-Blodgett method, self-assembly, and intercalation method have been investigated in this direction [5-8]. Since increasingly the components for the nanomaterials construction are organic molecules and their supramolecular complexes, it seems that there is no alternative to the intercalation method. This method is devoid of variability limitations in the choice of various hetero-ingredients and host-guest configurations problematic synthesis. The host-guest configurations systems are possible to achieve: directed changes of the initial atomic and molecular structure. Also, such systems are possible for synthesis in the intercrystalline field of host materials of chemicals, certain structures formation at the atomic and molecular level, and, in the future, the whole functional blocks.

The guest is under the influence of weak interactions with the host. Ionic-dipolar interactions, Van der Waals interactions, π-interactions, hydrogen bonding and hydrophobic effects are examples. The guest is a kind of matrix, that keeps its identity and exhibits quantum-size properties. The detected significant changes in the phase transition parameters for nanostructured substances [9], quantum enhancement of sensory sensitivity to external physical fields [10, 11] or a gigantic increase in the dielectric constant [12, 13] are examples of the nanoscale impact on the guest. At the same time, the magnitude and nature of these changes depend on the matrix kind, guest content, and also synthesis way.

The formation of more complex clathrate complexes such as subhost<host<guest>> is an interesting research area, which opens up new possibilities for designing heterostructured nanocomposites. Due to the intercalation technologies application and the use of inorganic matrices with 1D and 2D guest positions, it is possible to ensure the appropriate spatial arrangement providing the same time effective anticoagulation matrix isolation of supramolecular complexes and their properties stabilization [14, 15]. In the present case, the formation process of clathrate hierarchical structures gives the possibility to impose external physical fields, the action of which can lead to the supramolecular guest component ordering formation or change its properties. The work [16] is an example, in which by clathrate illumination during its formation it was possible to realize photoelectret polarization of the guest component, which allowed to obtain a colossal photodielectric effect.

This work's aim is to continue the study of complex clathrate complexes of the subhost<host<guest>> type and the effect of illumination on the photoelectric properties of the obtained clathrates.

2. MATERIALS AND RESEARCH METHODS

A clathrate of the subhost<host<guest>> hierarchical architecture, InSe<$CS(NH_2)_2$<$C_{14}H_{10}$>>, was formed for the research.

A semiconductor single crystal InSe was used as the matrix by the sub-host. The single crystal grown by the Bridgman-Stockbarger method has a pronounced layered structure and *n*-type conductivity (Fig. 1). Layered crystal is a promising thermoelectric material with a

high potential field value. Due to its structural features [17], it can be applied in various electronics areas [18, 19] and can be used as an electronically conductive semiconductor matrix with 2D guest positions. The last thing is very important in our case.

Thiourea ($CS(NH_2)_2$) is a supramolecular cavitand and it was the host (Fig. 2). This is possible due to strong intermolecular hydrogen bonds between acid protons of NH_2-groups and oxygen or sulfur atoms in neighboring molecules [20, 21]. The dipole moment of thiourea is $18.86 \cdot 10^{-30}$ C·m and the relative permittivity of thiourea is 2.224 [22]. The nonlinear optical properties of thiourea are currently widely used in the electronics industry, for example, as polarization filters, electronic optical gates, an electronic modulator, and as a component in electro-optical and electro-acoustic devices. In addition, thiourea is widely used in various electrochemical processes [23, 24].

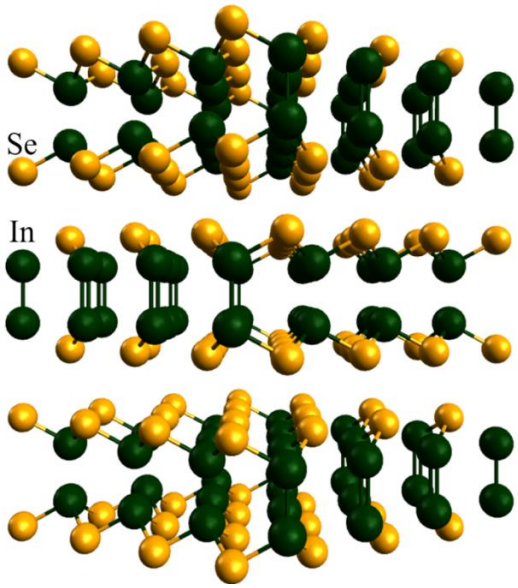

Fig. 1 – Spatial representation of the InSe structure

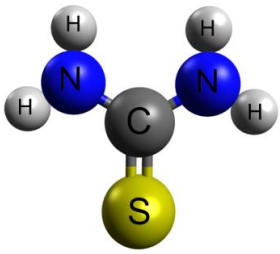

Fig. 2 – Molecular structure of thiourea

Anthracene ($C_{14}H_{10}$) was chosen as a guest (Fig. 3) [24, 25]. It is a well-known organic photoelectret whose properties in the macrostructured state are very well studied. Instead, changes in the photoelectret polarization mechanisms during the transition to the nanostructured state and the guest content in clathrates are practically not studied today.

The supramolecular compound $CS(NH_2)_2\langle C_{14}H_{10}\rangle$ was formed by mixing saturated solutions of the corresponding components in a molar ratio of 1:1. Ethyl alcohol of 96 % was used as a solvent for both substances.

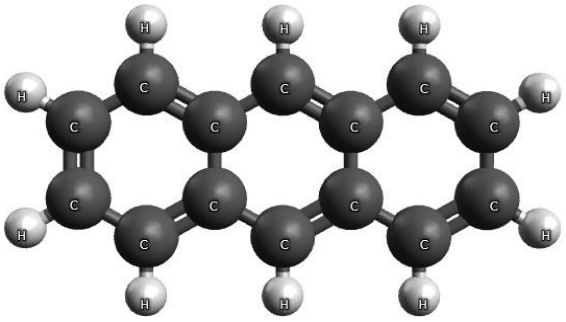

Fig. 3 – Molecular structure of anthracene

The InSe crystal matrix adaptation to the $CS(NH_2)_2\langle C_{14}H_{10}\rangle$ supramolecular complex insertion between the layers was realized by applying the intercalation-deintercalation three-stage crystal engineering technology detailly described in our previous works [26]. At the second stage end, the crystal matrix expansion of InSe single crystal was 4-fold. Ohmic contacts were deposited on the opposite faces of the crystal and the initial expanded matrix was studied.

The next step in the third technological stage was the supramolecular complex insertion by matrix dipping into the formed solution of thiourea and anthracene and keeping InSe single crystal in it for 24 h to ensure the intercalation process. Then the sample was taken out from the solution and the outer faces were rinsed. Then the sample was subjected to illumination and drying at the same time. Illumination during sample drying was used to ensure photoelectret polarization of the supramolecular component. For this purpose, the standard solar spectrum lamp imitator AM 1.5G with a total available power of 982 W/m^2 was used. The evaporation process with simultaneous illumination lasted for 6 h. The sample was illuminated in the direction perpendicular to the InSe single crystal layers' plane.

Impedance spectra were measured with the help of the measuring complex "AUTOLAB" of the company "ECO CHEMIE" (Netherlands) in the single crystal crystallographic *C* axis direction in the frequency range $10^{-3} \div 10^6$ Hz. Impedance spectra measurements were carried out under normal conditions, in a constant magnetic field (2.75 kOe) or under illumination (the same lamp was used as in the synthesis of clathrate). The action of the corresponding physical fields was focused in the direction of the measuring signal transmission. This measurement geometry was chosen for collinear action of the constant magnetic field or illumination and the measuring signal current.

Thermally stimulated discharge spectra in the short-circuited contacts mode under linear heating at a rate of 5 °C/min were measured to establish the impurity levels' electronic energy topology structure.

3. MATERIALS AND RESEARCH METHODS

Let us begin the analysis of the conductive properties of the initial 4-fold expanded InSe matrix and $InSe\langle CS(NH_2)_2\langle C_{14}H_{10}\rangle\rangle$ clathrate formed on its basis. Therefore, the frequency dependences of the real part of the complex impedance $\mathrm{Re}Z(\omega)$ measured for the initial and intercalated matrices are shown in Fig. 4.

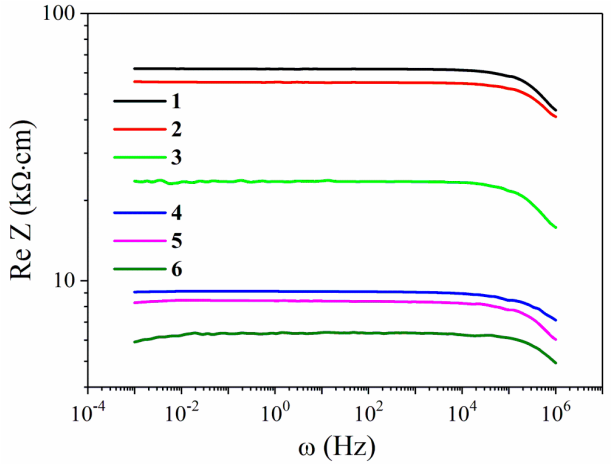

Fig. 4 – Frequency dependences of the real part of the specific complex impedance of the initial InSe matrix (1, 2, 3) and InSe<$CS(NH_2)_2$<$C_{14}H_{10}$>> clathrate (4, 5, 6). The measurements were carried out under normal conditions (1, 4), in a constant magnetic field (2, 5), and under illumination (3, 6)

Such an initial 4-fold expanded InSe matrix under normal measurement conditions is characterized by the resistance behavior of the charge transfer stage characteristic of this type of object. Re$Z(\omega)$ takes frequency-independent behavior in a wide frequency range, which indicates the main contribution to the conductivity of thermally excited current carriers (Fig. 4 curve 1). Starting from a frequency of 10^4 Hz, Re$Z(\omega)$ becomes frequency-dependent, which indicates the hopping conductivity activation of current carriers with energies close to the Fermi level E_F. The frequency-dependent conductivity, in this case, can be written in the following form:

$$\sigma(\omega) \equiv Re\hat{\sigma}(\omega) \sim \omega^n ,$$

where the exponent of degree n can take values in the range $0.64 \le n \le 1.0$. In this case, starting from the frequency of 10^4 Hz, the conductivity obeys the functional dependence $\sigma(\omega) \sim \omega^{0.8}$. The constant magnetic field applied during the measurement leads to a slight (within 12 %) decrease in the real part of the complex resistance ReZ (Fig. 4 curve 2) due to the Zeeman delocalization of the current carriers, without changing the behavior itself. Illumination leads to the ReZ decrease more than 2.5 times (Fig. 4 curve 3), which is expected concerning the photosensitivity of InSe single crystal. However, in the low-frequency part of the spectrum Re$Z(\omega)$, there are oscillations caused by the negative capacitance phenomena manifestation [27], which is the result of the processes of capture and holding of the current carriers by trap centers for a time commensurate with the period of the sinusoidal measuring signal. Taking into account that during the single crystal expansion, not each layer expansion occurs, but according to the stage ordering of each n-th layer [28], the initial 4-fold expanded matrix will present unexpanded packs of single crystal layers separated by an expanded layer. Trap centers will form in the expanded layers. Under the illumination influence, there are non-equilibrium carriers "throwing" into the formed in the extended areas resonance levels band, and their further release under the action of an alternating measuring signal.

The $CS(NH_2)_2$<$C_{14}H_{10}$> supramolecular complex insertion between the layers of the 4-fold expanded InSe matrix leads to a 6.85-fold decrease in ReZ. It should be noted that in previous studies [16, 29], the thiourea and anthracene components insertion separately between the layers of InSe single crystal under similar conditions has led to the resistance increase in both cases. In our case, the insertion of the supramolecular complex <$CS(NH_2)_2$<$C_{14}H_{10}$>> leads to an increase in the free charge carrier concentration due to the guest subsystem, which acts as an electron donor (Fig. 4, curve 4). Generally, the Re5(ω) behavior for InSe<$CS(NH_2)_2$<$C_{14}H_{10}$>> clathrate repeats the initial 4-fold expanded InSe matrix behavior. The constant magnetic field applied to InSe<$CS(NH_2)_2$<$C_{14}H_{10}$>> clathrate leads to a 10 % decrease in Re$Z(\omega)$ due to the Zeeman delocalization of current carriers. Under the illumination of InSe<$CS(NH_2)_2$<$C_{14}H_{10}$>> clathrate, we obtain a significant decrease in the photoresistive effect, as the resistance decrease is only 1.5 times. But more interesting is the frequency genesis change of the low-frequency part of Re$Z(\omega)$, which takes on a monotonically increasing character. This low-frequency behavior of Re$Z(\omega)$ can be related to the quantum photocapacitance manifestation [30], which can be caused by the energy spectrum discretization and finite tunneling times.

Using the theory of hopping conductivity proposed by M. Pollak and T.H. Geballe [31], which takes into account the charge carriers hopping between states localized in space due to their interaction with phonons. The result is the following expression for the real part of the conductivity:

$$\sigma(\omega) = \frac{\pi}{96} e^2 k_B T \alpha^{-5} N_F^2 \omega \left[ln\left(\frac{\nu_\Phi}{\omega} \right) \right]^4 , \qquad (1)$$

where e is the electron charge; N_F is the density of states at the Fermi level; α is the constant of the carrier localized wave function decrease; ν_Φ is the phonon frequency. The density of states at the Fermi level N_F was determined based on the equation (1) and experimentally measured values of $\sigma(\omega)$.

According to the theory of hopping conductivity on alternating current, the average hopping time τ of the carrier with phonon absorption or emission is determined by the expression:

$$\tau^{-1} = \nu_\Phi exp(-2\alpha R), \qquad (2)$$

where R is the hopping distance. Experimentally, τ^{-1} is the average frequency, at which the law $\omega^{0.8}$ is fulfilled. The average hopping distance R can be calculated by the formula after determining the value of τ^{-1} experimentally.

The scatter of trapped levels near the Fermi level J can be estimated by knowing the values of N_F and R from the relation

$$\frac{4}{3}\pi R^3 N_F \frac{1}{2} J = 1 . \qquad (3)$$

This, in turn, makes it possible to estimate the real density of deep traps N_t using the formula

$$N_t = N_F J \,. \quad (4)$$

The corresponding values obtained according to the presented calculations are given in Table 1. As we can see, the guest component insertion leads to an increase in the density of states at the Fermi level, a decrease in the average hopping distance, a decrease in the scatter of trap levels near the Fermi level and a greater increase in the density of deep trap centers. Generally, we obtain a sufficiently good correlation above mentioned current transmission mechanisms with theoretically calculated results.

Table 1 – Band spectrum parameters before and after insertion of <$CS(NH_2)_2$<$C_{14}H_{10}$>> into InSe

Structure	$N_F \cdot 10^{44}$, $J^{-1}m^{-1}$	$R \cdot 10^{-8}$, m	$J \cdot 10^{-23}$, J	$N_t \cdot 10^{22}$, m^{-3}
4-fold expanded InSe matrix	3.50	2.64	7.40	2.58
InSe< $CS(NH_2)_2$<$C_{14}H_{10}$>> clathrate	5.17	2.45	6.25	3.23

Thermally stimulated discharge currents of the initial 4-fold expanded InSe matrix and InSe<$CS(NH_2)_2$<$C_{14}H_{10}$>> clathrate formed on its basis were measured to confirm the obtained results experimentally (Fig. 5). The homo-charge relaxation is typical for both spectra. It has a correlation with the impedance studies results because the matrix and the supramolecular guest component are characterized by *n*-type conductivity. Both spectra are characterized by broad bands with the localized defect states quasi-continuous spectrum in this system. The change in the energy structure of defects after <$CS(NH_2)_2$<$C_{14}H_{10}$>> supramolecular guest insertion into the 4-fold expanded InSe matrix is visible.

It is obvious that the behavior of the imaginary component of the complex impedance – Im$Z(\omega)$ will change after <$CS(NH_2)_2$<$C_{14}H_{10}$>> supramolecular guest insertion into the 4-fold expanded InSe matrix. The corresponding hodographs are shown in Fig. 6. Regardless of the measurement conditions, the main relaxation maximum for the initial 4-fold expanded InSe matrix (Fig. 6, curves 1-3) is outside the measuring frequency range.

The guest component insertion and the GaSe<$CS(NH_2)_2$<$C_{14}H_{10}$>> clathrate formation lead to the main relaxation maximum shift towards lower frequencies, which allows it to be fixed in a frequency vicinity of $8 \cdot 10^5$ Hz of the measuring range. This illustrates the contribution of supramolecular guest component carriers with significantly lower mobility. The application of a constant magnetic field and illumination does not lead to the main relaxation maximum additional shift, and therefore does not influence the mobility of the carriers. However, when a constant magnetic field is applied, the main relaxation maximum increases intensity, which is the opposite behavior compared to the initial 4-fold expanded InSe matrix and indicates the peculiarities of the Zeeman effect for the guest subsystem. As a confirmation of this, illumination does not lead to significant changes in the main relaxation maximum intensity.

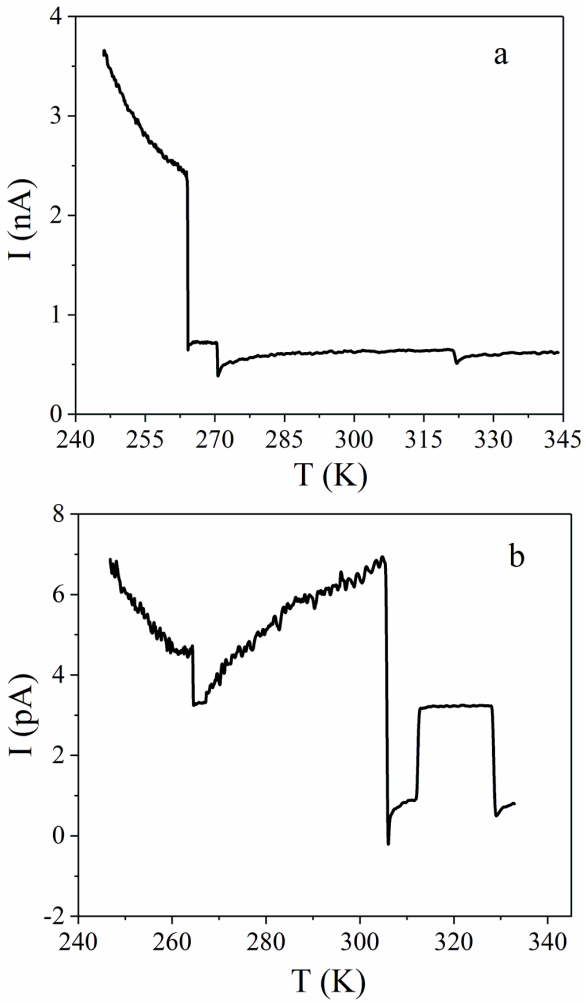

Fig. 5 – Thermally stimulated discharge current spectra measured for the 4-fold expanded InSe matrix (a) and InSe<$CS(NH_2)_2$<$C_{14}H_{10}$>> clathrate (b)

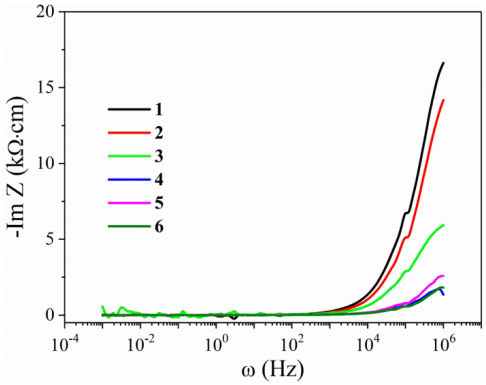

Fig. 6 – Frequency dependences of the imaginary component of the specific complex impedance of the 4-fold expanded InSe matrix (1, 2, 3) and InSe<$CS(NH_2)_2$<$C_{14}H_{10}$>> clathrate (4, 5, 6). Measurements were carried out under normal conditions (1, 4), in a constant magnetic field (2, 5) and under illumination (3, 6)

The confirmation of the above-mentioned statements is obtained by displaying the Nyquist plots for the initial 4-fold expanded InSe matrix and InSe<$CS(NH_2)_2$<$C_{14}H_{10}$>> clathrate shown in Fig. 7. The hodographs have the incomplete semicircles form, which is caused by the frequency limitation of the

measuring equipment. The equivalent circuit diagram can be presented in the form shown in Fig. 8. There, the first high-frequency parallel branch R‖CPE (where CPE is a capacitive-type constant phase element [6]) simulates the current transmission through the unexpanded packages of the InSe single crystal.

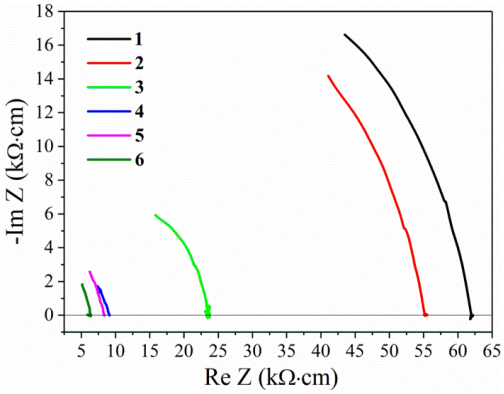

Fig. 7 – Nyquist plots of the 4-fold expanded InSe matrix (1, 2, 3) and InSe<CS(NH$_2$)$_2$<C$_{14}$H$_{10}$>> clathrate (4, 5, 6). Measurements were carried out under normal conditions (1, 4), in a constant magnetic field (2, 5) and under illumination (3, 6)

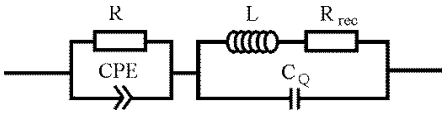

Fig. 8 – Equivalent circuit scheme

The second branch, the low-frequency component $C_Q‖R_{rec}L$, models the current transmission through extended layers of the semiconductor matrix. Here, R_{rec} is the recombination resistance, which models the barrier for charging C_Q, L is the inductance, C_Q is the quantum capacitance [31], which is described by the equation $C_Q = e^2 dn / dE_{Fn}$, where n is the electron concentration, E_{Fn} is the position of the electronic quasi-Fermi level. The admittance for the last branch in the low-frequency region can be written as:

$$Y(\omega) = \frac{1}{R_{rec}} - i\omega C, \qquad (5)$$

where $C = C_L - C_Q$, $C_L = L / R_{rec}^2$.

According to equation (5), at very low frequencies ($\omega < \frac{1}{R_{rec}C}$) the impedance of the last branch of the equivalent circuit for the illuminated nanohybrid is a parallel connection of the recombination resistance R_{rec} and a constant negative capacitance C. Obviously, when $C_L > C_Q$, the low-frequency branch enters the IV-inductive quadrant, showing an inductive response. Instead, when the situation is opposite to $C_Q > C_L$, the low-frequency branch lies parallel to the abscissa axis and is oriented towards a decrease in value.

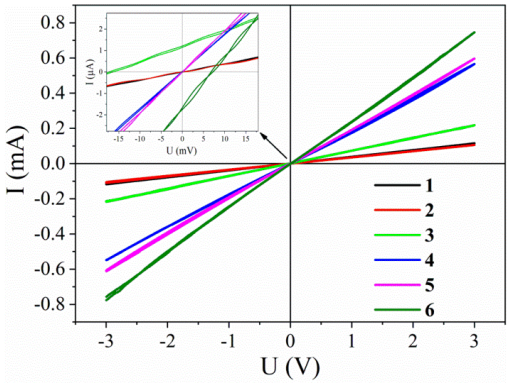

Fig. 9 – Current-voltage characteristics measured for the initial InSe matrix (1, 2, 3) and InSe<CS(NH$_2$)$_2$<C$_{14}$H$_{10}$>> clathrate (4, 5, 6). Measurements were carried out under normal conditions (1, 4), in a constant magnetic field (2, 5), and under illumination

Current-voltage characteristics for the initial InSe matrix and InSe<CS(NH$_2$)$_2$<C$_{14}$H$_{10}$>> clathrate are linear, but not all pass through the coordinate center (Fig. 9). So, for measurements under illumination for the initial 4-fold expanded InSe matrix, the current-voltage characteristic crosses the voltage axis at – 16.5 mV, and for InSe<CS(NH$_2$)$_2$<C$_{14}$H$_{10}$>> clathrate, crosses at + 7 mV. In the case of the photoelectric effect for the initial crystal matrix, there is nothing unusual since the chosen semiconductor is photosensitive. However, an interesting fact is that for clathrate, the photoelectric effect changes the sign to the opposite one, from which it is possible to assume that the guest component generates photocurrent of the opposite sign of + 23.5 mV.

4. CONCLUSIONS

1. InSe<CS(NH$_2$)$_2$<C$_{14}$H$_{10}$>> clathrate of the sub-host<host<guest>> hierarchical architecture with the imposition of illumination during the preparation was synthesized for the first time.
2. The formed InSe<CS(NH$_2$)$_2$<C$_{14}$H$_{10}$>> clathrate is characterized by relaxation of homo-charge and broad bands with the localized defect states quasi-continuous spectrum.
3. The energy spectrum discretization of InSe<CS(NH$_2$)$_2$<C$_{14}$H$_{10}$>> clathrate and carrier tunneling through the potential barrier formed at the hetero-boundary leads to the appearance of photoinduced quantum capacitance.
4. Considering that the photocurrent of the initial 4-fold expanded InSe matrix is – 16.5 mV and for InSe<CS(NH$_2$)$_2$<C$_{14}$H$_{10}$>> clathrate it is equal to + 7 mV, it is possible to state that the insertion of the guest component leads to the formation of photocurrent that is + 23.5 mV.

REFERENCES

1. S.-M. Paek, J.-M. Oh, J.-H. Choy, *Chem. – An Asian J.* **6** No 2, 324 (2010).
2. C. Tan, X. Cao, X.-J. Wu, Q. He, J. Yang, X. Zhang, H. Zhang, *Chem. Rev.* **117** No 9, 6225 (2017).
3. S.M. Oh, S.B. Patil, X. Jin1, S.-J. Hwang, *Chem. – A Eur. J.* **24** No 19, 4757 (2018).
4. T. Gu, X. Jin, S. Park, M.G. Kim, S. Hwang, *Adv. Sci.* **8** No 7, 2004530 (2021).
5. H. Biederman, O. Kylian, M. Drabik, A. Choukourov, O. Polonskyi, Solar, *Surf. Coat. Technol.* **211**, 127 (2012).
6. S.A. Hussain, B. Dey, D. Bhattacharjee, N. Mehta, *Heliyon* **4** No 12, e01038 (2018).
7. W. Tian, A. Vahid Mohammadi, Z. Wang, L. Ouyang, M. Beidaghi, M.M. Hamedi, *Nat. Commun. Rev.* **10** No 1, 2558 (2019).
8. M.S. Stark, K.L. Kuntz, S.J. Martens, S.C. Warren, *Adv. Mater.* **31**, 1808213 (2019).
9. J.F. Ihlefeld, D.T. Harris, R. Keech, J.L. Jones, J.-P. Maria, S. Trolier-McKinstry, *J. Am. Ceram. Soc.* **99** No 8, 2537 (2016).
10. A. Płomińska, I. Weymann, *EPL (Europhysics Letters)*, **125** No 1, 18004 (2019).
11. J. Zeng, F. Xie, K.-Q. Chen, *Carbon* **98**, 607 (2016).
12. V. Maksymych, D. Całus, F. Ivashchyshyn, A. Pidluzhna, P. Chabecki, R. Shvets, *Appl. Nanosci.* **12**, 1147 (2021)
13. I.I. Grygorchak, F.O. Ivashchyshyn, A.K. Borysiuk, R.Ya. Shvets, Yu.O. Kulyk, *Radio Electronics, Computer Science, Control* **3**, 7 (2017).
14. J.-H. Choy, *J. Phys. Chem. Solid.* **65** No 2-3, 373 (2004).
15. G. Choi, S. Eom, A. Vinu, J.-H. Choy, *Chem. Record* **18** No 7-8, 1033 (2018).
16. F.O. Ivashchyshyn, O.V. Balaban, I.I. Grygorchak, *J. Nano-Electron. Phys.* **8** No 4, 04015 (2016).
17. I. Mora-Seró, J. Bisquert, F. Fabregat-Santiago, G. Garcia-Belmonte, G. Zoppi, K. Durose, S.J.C. Irvine, *Nano Lett.* **6** No 4, 640 (2006).
18. N.T. Hung, A.R.T. Nugraha, R. Saito, *Appl. Phys. Lett.* **111** No 9, 092107 (2017).
19. A.K. Geim, I.V. Grigorieva, *Nature* **499** No 7459, 419 (2013).
20. F. Huang, Z. Li, H. Jiang, *Cailiao Baohu* **30**, 23 (1997).
21. T. Pluta, A.J. Sadlej, *J. Chem. Phys.* **114** No 1, 136 (2001).
22. C. Puzzarini, *J. Phys. Chem. A* **116**, 4381 (2012).
23. S. Kausar, Ali Altaf Ataf, M. Hamayun, A. Badshah, A. Razzaq, *Studies of Ferrocenyl Ureas and Thioureas* (2020).
24. BX. Shang, Z. Yang, J. Fu, P. Zhao, X. Xu, *Sensors* **15** No 11, 28166 (2015).
25. A.J. Goshe, I.M. Steele, C. Ceccarelli, A.L. Rheingold, B. Bosnich, *Proc. Nat. Acad. Sci.* **99** No 8, 4823 (2002).
26. I. Grygorchak, F. Ivashchyshyn, P. Stakhira, R.R. Reghu, V. Cherpak, J.V. Grazulevicius, *J. Nanoelectron. Optoelectron.* **8**, 292 (2013).
27. P. Kostrobij, I. Grygorchak, F. Ivashchyshyn, B. Markovych, O. Viznovych, M. Tokarchuk, *J. Phys. Chem. A* **122** No 16, 4099 (2018).
28. S.A. Safran, *Solid State Phys.: Adv. Res. Appl.* **40**, 246 (1987).
29. I.I. Hryhorchak, F.O. Ivashchyshyn, Yu.O. Kulyk, O.I. Hryhorchak, *Zhurnal fizyky ta inzheneriyi poverkhni*, **2** No 1, 49 (2017).
30. F.O. Ivashchyshyn, I. Grygorchak, M.I. Klapchuk, *Nanosystems, Nanomaterials, Nanotechnologies* **13** No 3, 403 (2015).
31. M. Pollak, T.H. Geballe, *Phys. Rev.* **6**, 1743 (1961).

Електропровідні та поляризаційні властивості клатрату InSe<CS(NH$_2$)$_2$<C$_{14}$H$_{10}$>>

В. Максимич[1], Д. Цалус[2], Д. Матулка[1], П. Хабецкі[2], Р. Швець[1], Н. Покладок[1], Ф. Іващишин[1,2]

[1] *Інститут прикладної математики та фундаментальних наук, Національний університет "Львівська політехніка", вул. Степана Бандери, 12, 79013 Львів, Україна*

[2] *Електротехнічний факультет, Ченстоховський політехнічний університет, вул. Я.Г. Домбровського, 69, 42-201 Ченстохова, Польща*

Інтеркаляційним методом сформовано під дією світла 2D структуру ієрархічної будови типу субгосподар<господар<гість>> – клатрат InSe<CS(NH$_2$)$_2$<C$_{14}$H$_{10}$>>. В даному випадку як напівпровідникову 2D матрицю використано шаруватий монокристал InSe, тіосечовина (CS(NH$_2$)$_2$) виступала як супрамолекулярний кавітанд, а антрацен (C$_{14}$H$_{10}$) – як фотоелектрет. Освітлення при синтезі використовувалося для фотоелектретизації антрацену. Методом імпедансної спектроскопії було досліджено електропровідні та поляризаційні властивості клатрату InSe<CS(NH$_2$)$_2$<C$_{14}$H$_{10}$>>. В результаті зафіксовано прояв фотоіндукованої квантової ємності, природа якої пов'язана із дискретизацією енергетичного спектру та скінченністю часів тунелювання. За результатами дослідження спектрів термостимульованого розряду встановлено, що клатрату InSe<CS(NH$_2$)$_2$<C$_{14}$H$_{10}$>> властива релаксація гомозаряду та широкі смуги із квазінеперервним спектром локалізованих станів. Поведінка ВАХ свідчить про прояв фото-ЕРС величиною + 23,5 мВ.

Ключові слова: InSe, Тіосечовина, Антрацен, Клатрат, Імпедансна спектроскопія, Квантова ємність, Фото-ЕРС.